Manuscript submitted to
AIMS' Journals
Volume **X**, Number **0X**, XX **200X**

Website: http://AIMsciences.org

pp. **X–XX**

PARITY SYMMETRY IN MULTI-DIMENSIONAL SIGNALS

Gerald Sommer and Di Zang

Institute of Computer Science
Christian-Albrechts-University
24118, Kiel, Germany

(Communicated by Aim Sciences)

Abstract. Parity symmetry is an important local feature for qualitative signal analysis. It is strongly related to the local phase of the signal. In image processing parity symmetry is a cue for the line-like or edge-like quality of a local image structure. The analytic signal is a well-known representation for 1D signals, which enables the extraction of local spectral representations as amplitude and phase. Its representation domain is that of the complex numbers. We will give an overview how the analytic signal can be generalized to the monogenic signal in the nD case within a Clifford valued domain. The approach is based on the Riesz transform as a generalization of the Hilbert transform with respect to the embedding dimension of the structure. So far we realized the extension to 2D and 3D signals. We learned to take advantage of interesting effects of the proposed generalization as the simultaneous estimation of the local amplitude, phase and orientation, and of image analysis in the monogenic scale-space.

1. **Introduction.** Image analysis based on local spectral representations, that is amplitude and phase, has been a well-known method of signal processing for years [24]. The aim is to assign a structural or/and geometric interpretation to an image point. We call that task of computing the split of identity. This obviously only makes sense with respect to the coupling of a pixel with its immediate environment and can, thus, be realized by local operators. Because local structure is specific for a certain scale it lives at, a multi-resolution scheme is recommended. Besides being bandpass filters, the operators have to be quadrature pairs [2] to make the local symmetry accessible. In the multi-dimensional case, local symmetry is entangled with local orientation. Regrettably, until recently no construction rule for isotropic multi-dimensional quadrature filter pairs was known. Therefore, efficient steering [22, 39] of the orientations of directed quadrature filters was a matter of research for several years with the aim of disentangling local spectral features and orientation, and for designing artificial visual architectures [21].

Our group also spent a lot of work with qualifying steerable filter design [36, 44, 48]. But in parallel work we were looking for a more general solution to extract local spectral representations in a rotation invariant manner. Our approach differs from other efforts in either linear [25, 6] or nonlinear [31] schemes of extending the analytic signal to higher dimensions. This paper reports on the common design principles of the class of isotropic band-pass quadrature filters which work on signals

2000 *Mathematics Subject Classification.* Primary: 58F15, 58F17; Secondary: 53C35.
Key words and phrases. Parity symmetry, local phase, monogenic scale-space.

of dimension one, two or three. But the results can be generalized to any dimension. The way we have gone is a generalization of the analytic signal which cannot be found in the domain of complex numbers. Instead, to provide a more powerful algebraic system, the modelling of our problem at hand has to be done best in Clifford algebra or geometric algebra, respectively [27, 34].

A great bulk of results goes back to the PhD thesis of M. Felsberg [13]. For people working in signal theory or image processing the chosen approach may be a new one. But only the recent results in Clifford analysis [3, 45, 32] enabled us to understand correctly the underlying deep representation problems we met and to close the representation gap coherently. Hence, our approach of extracting the local parity symmetry of a multi-dimensional signal must be seen as an application of Clifford harmonic analysis.

We will show that the approach we are presenting solves the problem of computing local spectral representations in the case of multi-dimensional signals in a rigorous and general way. We call that gained signal representation the monogenic signal [16]. To mention only some main results: First, the isotropic quadrature filters enable to measure local spectral representations in a rotation invariant manner and they deliver the exact orientation information nearly for free, completely without steering. Second, the even more fundamental result is a new scale-space concept which, in contrast to the Gaussian scale-space not only relates the signal intensity to the scale of the operators, but unifies scale concepts of local amplitude, phase, and orientation in one single framework, the monogenic scale-space [20]. Third, the coupling of the monogenic signal representation with the second fundamental theorem of differential geometry enables in the 2D case the handling of all intrinsic dimensions. The monogenic curvature tensor delivers the monogenic signal as a special case for i1D structures. Finally, the generalized monogenic curvature scale-space is the most general framework for local representation of a 2D signal in a scale-space concept.

2. **Foundations of Signal Theory.**

2.1. **Local Spectral Representations.**

In this subsection we want to summarize the relations of the term parity symmetry in the title of this paper with the task of computing the split of identity. Parity refers to the invariance of a process with respect to a reflection operation. Parity symmetry is understood as the structural feature of a signal we derive from the local phase. That is, phase analysis results in a mapping of a signal to a basis spanned by even and odd symmetry.

In the case of a 1D signal $f : \mathbb{R} \longrightarrow \mathbb{R}$ this mapping is a rather simple task. The theoretic approach is to compute the analytic signal $f_A : \mathbb{R} \longrightarrow \mathbb{C}$ [23] in either spatial or Fourier domain. Let $\mathcal{F}$ be the Fourier transform, then $F_A(u) = \mathcal{F}\{f_A(x)\}$ with

$$f_A(x) = f(x) + j f_H(x) \tag{1}$$

$$F_A(u) = F(u) + j F_H(u) = (1 + \text{ sign } (u))F(u). \tag{2}$$

The components f and f_H of the complex valued signal f_A are phase shifted by $-\frac{\pi}{2}$, they are in quadrature phase. The imaginary completion f_H is computed from the real signal f by applying the Hilbert transform $\mathcal{H}$ in either spatial or Fourier

domain, $f_H(x) = (f * PVh)(x)$ with PV denoting the principal value,

$$h(x) = \frac{1}{\pi x} \quad \text{and} \quad H(u) = -j \text{ sign } (u). \tag{3}$$

Then the local energy $e(x)$ and the local phase $\phi(x)$, respectively are defined by

$$e(x) = f^2(x) + f_H^2(x) \tag{4}$$

$$\phi(x) = \arg f_A(x). \tag{5}$$

In the case that the local energy exceeds a certain threshold of significance, then the parity symmetry of the local phase enables a local structure analysis. The following ideal cases occur: peak: $\phi(x) = 0$, pit: $\phi(x) = \pi$, decreasing slope: $\phi(x) = \frac{\pi}{2}$, increasing slope: $\phi(x) = -\frac{\pi}{2}$. Both peak and pit indicate even symmetry, while slopes indicate odd symmetry. In the case of a real signal a symmetry somewhere in between may be assigned to a certain location. Because the Hilbert transform is an allpass operator, in practice quadrature filter pairs [24] are preferred. Being bandpass filters, they have to guarantee the quadrature phase relation only within a passband. This is achieved by coupling two filters of even and odd symmetry according to

$$h_q(x) = h_e(x) + jh_o(x). \tag{6}$$

The Gabor filter [23] is a widely used example. Convolution of f with each filter of the quadrature pair $\{h_e, h_o\}$ results in the complex valued output function

$$g(x) = g_e(x) + jg_o(x). \tag{7}$$

In that case the real axis in the complex domain indicates pure even symmetry and the imaginary axis indicates pure odd symmetry. Gabor filters are used as standard quadrature filters in image analysis [24]. Because their lack of rotation invariance, they are applied as oriented filters.

While in 1D things are simple, we will get all possible couplings of symmetry in the multi-dimensional case. This causes the lack of a general multi-dimensional phase model. At this point the term intrinsic dimension [53] of a signal comes into play. It is related to the geometric interpretation of a local structure. We have to distinguish between the global embedding dimension n of a signal and its (local) intrinsic dimension d. The term intrinsic dimension as used in image processing corresponds to the term codimension in mathematics: If $S \subset \mathbb{R}^n$ is a subspace, then

$$d(S) = \text{ codim } S = n - \text{ dim } S. \tag{8}$$

In the 1D case, a point $x \in \mathbb{R}$ is of topological dimension [28] zero and of intrinsic dimension one. A signal, which is constant for all $x \in \mathbb{R}$, is of intrinsic dimension zero.

In the 2D case of $f(\mathbf{x})$, $\mathbf{x} \in \mathbb{R}^2$, we meet the following intrinsic d-dimensional signals (idD signals):

$$f(\mathbf{x}) \in \begin{cases} \{\text{i0D}\} & \text{if } f(\mathbf{x}) = \text{ const for all } \mathbf{x} \in \mathbb{R}^2 \\ \{\text{i1D}\} & \text{if } f(\mathbf{x}) = f(\alpha x + \beta y)\ ,\ \alpha \neq 0 \text{ or } \beta \neq 0 \\ \{\text{i2D}\} & \text{else} \end{cases} \tag{9}$$

While for a constant signal $f(\mathbf{x}) \in \{\text{i0D}\}$ we get $e(\mathbf{x}) = 0$, for $f(\mathbf{x}) \in \{\text{i1D}\}$ we get $e(\mathbf{x}) = 0$ only in the orientation $\theta = \arctan \frac{\beta}{\alpha}$ and $e(\mathbf{x}) \neq 0$ for all other angles different from θ. In the case of i2D signals points are the considered subspaces

$S \subset \mathbb{R}^2$. There exists no general rule for finding a single orientation which enables phase analysis. But nevertheless, by assuming certain signal models, also in the i2D case a phase can be defined. So i1D signals in $\mathbb{R}^n$ concern the important case of transferring the 1D concepts of symmetry analysis to higher dimensions. If $n = 2$ and $d = 1$, even symmetry is a feature of lines and odd one such of edges. Because we do not know their orientation in advance, orientation steering [22] comes into play. We will show for the cases $n = 2, 3$ and $d = 1$, how steering can be prevented and how this emerges coherently from the case $n = 1$. The more demanding task of analysing i2D signals in image processing, see [13, 31], is related to problems of corner detection or junction classification. From our contemporary point of view that intensively investigated area of research seems to be not generally solvable. But we will give a sketch of preliminary results for i2D signals concerning the case of two (not necessarily perpendicular) crossing i1D structures in section 4.5, which are based on a monogenic curvature tensor representation. This will enable us in image analysis to apply the well-known approach of differential geometry, enriched by a local spectral analysis in a monogenic framework.

As we will show, also in the 3D case the presented method works for i1D signals, but these are now planar structures.

2.2. **Global Spectral Representations.** If phase analysis is done by linear and shift invariant (LSI) filters, it must have a representation also in the Fourier domain. It is well-known [24] that any real function $f : \mathbb{R}^n \longrightarrow \mathbb{R}$ at any location $\mathbf{x} \in \mathbb{R}^n$ may be decomposed by reflection into an even and an odd part,

$$f(\mathbf{x}) = f_e(\mathbf{x}) + f_o(\mathbf{x}). \tag{10}$$

A real function is of even symmetry (parity invariance) if $f(-\mathbf{x}) = f(\mathbf{x})$ and of odd symmetry (parity variance) if $f(-\mathbf{x}) = -f(\mathbf{x})$ for all $\mathbf{x} \in \mathbb{R}^n$. Only in the case of a 1D function, the Fourier transform preserves that symmetry decomposition in an integral manner because of the parity symmetry properties of its basis functions

$$Q(u, x) = \exp(-j2\pi ux) = \cos(2\pi ux) - j \sin(2\pi ux). \tag{11}$$

Hence,

$$F(u) = F_e(u) + F_o(u) \tag{12}$$

for all $u \in \mathbb{R}$ with $F_e = \mathcal{F}\{f_e\}$, $F_o = \mathcal{F}\{f_o\}$, and $F_R = F_e$ is the real spectrum and $F_I = -jF_o$ is the imaginary spectrum. The amplitude spectrum $A(u) = |F(u)|$ is of even symmetry and the phase spectrum $\Phi(u) = \arg F(u)$ is of odd symmetry.

Quite different is the situation already in the 2D case. Although in that case we have also a parity symmetry in the Fourier domain, this differs from that in the spatial domain. Independent of the dimension of a real signal its complex Fourier spectrum is of Hermitian symmetry, that is

$$F(-\mathbf{u}) = F^T(\mathbf{u}), \tag{13}$$

from which immediately follows that the real part is even and the imaginary part is odd. Let

$$\begin{aligned} Q(\mathbf{u}, \mathbf{x}) &= \exp(-j2\pi \mathbf{u} \cdot \mathbf{x}) = \exp(-j2\pi(ux + vy)) \\ &= \exp(-j2\pi ux)\ \exp(-j2\pi vy)) \end{aligned} \tag{14}$$

for $\mathbf{x}$, $\mathbf{u} \in \mathbb{R}^2$ be the basis functions of the 2D Fourier transform,

$$F(\mathbf{u}) = F_{ee}(\mathbf{u}) + F_{oo}(\mathbf{u}) + F_{eo}(\mathbf{u}) + F_{oe}(\mathbf{u}). \tag{15}$$

Then

$$F_R(\mathbf{u}) = F_{ee}(\mathbf{u}) + F_{oo}(\mathbf{u}) \ , \quad F_I(\mathbf{u}) = -j \left(F_{eo}(\mathbf{u}) + F_{oe}(\mathbf{u}) \right) \tag{16}$$

as a result of the algebraic properties of the 2D basis functions (and similarly in the case of any dimension $n > 1$). Here (ee) means even symmetry with respect to both x and y, and so forth. Hence, we get no access to the single symmetry concepts in 2D signals by analysing the 2D Fourier spectrum. There exists no 2D phase representation in the complex domain which enables to represent all the possible interplays of 1D symmetries in local neighborhoods. To overcome that problem, we studied the quaternionic Fourier transform for 2D signals and in general Clifford valued Fourier transforms [5] of dimension 2^n for n- dimensional signals. The idea was that each coordinate of a signal should be represented by its own complex domain and their relations by certain additional DOFs of the chosen algebra. Although that was insofar the right way, as we could explicitly represent the symmetries of the single coordinates and some symmetries of their combination, the approach had the drawback of being not rotation invariant. This became especially obvious in the case of the designed quaternionic analytic signal [6] and quaternionic Gabor filters [7] as quadrature filter quadruples.

At this point two conclusions have to be drawn. First, it seems to be hopeless to design a Fourier transform in an algebraic domain as huge as ever to make explicit all possible combinations of parity symmetries we can meet already in 2D signals. Therefore, we concentrated to the problem of specifying the geometry, that is the orientation, of local intrinsic 1D structures in 2D or 3D images together with the local spectral features. Second, the missed rotation invariance of the quaternionic analytic signal has its reason in the use of line symmetry (reflections at coordinate axes) for the parity decomposition of the signal. Instead, we have to consider point symmetry to design an isotropic generalization of the Hilbert transform respectively an isotropic filter pair in quadrature phase. This is independent of the Fourier transform because the nD Fourier transform is both Cartesian and isotropic at the same time as a result of the rotation invariance of the scalar product $(\mathbf{x} \cdot \mathbf{u})$ of the basis functions.

3. **Foundations of Geometric Algebra.**

3.1. **Geometric Algebras of Euclidean Spaces.** Geometric algebras constitute a rich family of algebras as generalizations of vector algebra [27]. Their advantages in comparison to vector algebra result from a powerful subspace structure which, in contrast to subspaces of a vector space, are not restricted to interpretations within set theory but have geometric interpretations. These subspaces are called blades. In general, a geometric algebra (GA) $\mathbb{R}_{p,q,r}$ is a linear space of dimension 2^n, $n = p+q+r$, which results from a vector space $\mathbb{R}^{p,q,r}$. We call (p, q, r) the signature of the quadratic space over a vector space of dimension n. It indicates the number $p/q/r$ of unit vectors $\mathbf{e}_i$ which square to $1/-1/0$, respectively. By choosing the right signature, the GA will take on certain (geometric) properties which enables adaption of the embedding framework to the task at hand, see e.g. [43]. With our recent research in computer vision [42] we enforced for instance the use of the conformal GA $\mathbb{R}_{4,1}$ in the area of robot vision for modelling the (homogeneous) conformal geometry of the Euclidean space $\mathbb{R}^3$.

But for the problems we want to solve here, we only need the Euclidean GAs $\mathbb{R}_2$, $\mathbb{R}_3$, and $\mathbb{R}_4$ over the Euclidean spaces $\mathbb{R}^2$, $\mathbb{R}^3$, and $\mathbb{R}^4$, respectively. In these

cases we have $n = p$. We will not go much into details. A good source for studies of these Euclidean GAs is [34]. The chosen dimensions of the vector spaces result from the fact that we need an $(n+1)$-dimensional vector space for embedding our n-dimensional signals. Some more subspaces in comparison to the original n-dimensional one are needed to model operators and filters acting on the signal and to have enough DOFs for modelling all the features we want to extract locally from the signal.

The basic product of a GA is the geometric product, indicated by juxtaposition of the operands. This product is associative and non-commutative. There can be formulated a lot of other product forms too, as the outer product ($\wedge$) and the inner product ($\cdot$). Let $\mathbf{a},\ \mathbf{b} \in \mathbb{R}^n$ be two vectors, $\mathbb{R}^n \equiv \langle \mathbb{R}_n \rangle_1$, then their geometric product,

$$\mathbf{ab} = \frac{1}{2}(\mathbf{ab} + \mathbf{ba}) + \frac{1}{2}(\mathbf{ab} - \mathbf{ba}) \tag{17}$$

$$= \mathbf{a} \cdot \mathbf{b} + \mathbf{a} \wedge \mathbf{b} = \langle \mathbf{ab} \rangle_0 + \langle \mathbf{ab} \rangle_2 = \alpha + A_2,$$

results in the sum of a scalar $\alpha \in \langle \mathbb{R}_n \rangle_0$ and a bivector $A_2 \in \langle \mathbb{R}_n \rangle_2$. Here $\langle \cdot \rangle_k$ indicates the grade k part of the algebraic entity. A blade of grade k, a k-blade B_k, results from the outer product of k independent vectors $\{\mathbf{a}_1, \cdots, \mathbf{a}_k\} \in \mathbb{R}^n$,

$$B_k = \mathbf{a}_1 \wedge ... \wedge \mathbf{a}_k = \langle \mathbf{a}_1 ... \mathbf{a}_k \rangle_k. \tag{18}$$

There are $l_k = \binom{n}{k}$ different blades of grade k, hence $\sum_{k=0}^{n} l_k = 2^n$ is the dimension of GA. Unit blades of grade k, $I_k \equiv \mathbf{e}_{i_1 ... i_k} = \mathbf{e}_{i_1} \wedge ... \wedge \mathbf{e}_{i_k}$, with $1 \leq i_1 < \ldots < i_k \leq n$ are given by the outer product of k unit vectors of $\mathbb{R}^n$. They define the direction of a blade. The unit blade of grade n, I_n, is called unit pseudoscalar. It is important for mapping a multivector A to its dual one, A^*, hence, changing its basis within the GA by the inner product

$$A^* = A \cdot I_n^{-1}. \tag{19}$$

If $A \in \langle \mathbb{R}_n \rangle_k$, then $A^* \in \langle \mathbb{R}_n \rangle_{n-k}$. Let A_k be a k-vector of $\mathbb{R}_n, A_k = a_1 \ldots a_k$. Then the main anti-automorphism of $\mathbb{R}_n$, also called the reversion, is defined by $\widetilde{A}_k = a_k \ldots a_1$ and the main involution of $\mathbb{R}_n$, also called the parity conjugation is defined by $\widehat{A}_k = (-1)^k a_1 \ldots a_k$, see [26]. A multivector A is called even if $\widehat{A} = A$ and is called odd if $\widehat{A} = -A$.

Let us give a short view on the bases of $\mathbb{R}_2$ and $\mathbb{R}_3$:

1. $\dim(\mathbb{R}_2) = 4$
   $\text{basis}(\mathbb{R}_2) = \{\mathbf{e}_0,\ \mathbf{e}_1,\ \mathbf{e}_2,\ \mathbf{e}_{12}\}$
   $\mathbf{e}_0 \equiv 1,\ \mathbf{e}_{12} \equiv I_2,\ \mathbf{e}_0^2 = \mathbf{e}_1^2 = \mathbf{e}_2^2 = 1,\ \mathbf{e}_{12}^2 = -1$

2. $\dim(\mathbb{R}_3) = 8$
   $\text{basis}(\mathbb{R}_3) = \{\mathbf{e}_0,\ \mathbf{e}_1,\ \mathbf{e}_2,\ \mathbf{e}_3,\ \mathbf{e}_{23},\ \mathbf{e}_{31},\ \mathbf{e}_{12},\ \mathbf{e}_{123}\}$
   $\mathbf{e}_0 \equiv 1,\ \mathbf{e}_{123} \equiv I_3,\ \mathbf{e}_0^2 = \mathbf{e}_1^2 = \mathbf{e}_2^2 = \mathbf{e}_3^2 = 1,$
   $\mathbf{e}_{23}^2 = \mathbf{e}_{31}^2 = \mathbf{e}_{12}^2 = -1,\ \mathbf{e}_{123}^2 = -1.$

In $\mathbb{R}_4$ we can proceed similarly that way. But there are remarkable differences. Only to mention some: First, $I_4^2 = 1$ and second, the dual of a bivector is a bivector again. But also the geometry in $\mathbb{R}_4$ is hardly to imagine, see [34]. While in both $\mathbb{R}_2$ and $\mathbb{R}_3$ a bivector represents a plane, in $\mathbb{R}_4$ this is not generally the case. Also the rotation of a 4-ball in $\mathbb{R}_4$ happens quite different to that of a 3-ball in $\mathbb{R}_3$ or to that of a 2-ball in $\mathbb{R}_2$.

3.2. **Spinors in Euclidean Spaces.** We want to save as many concepts as possible from complex valued signal processing to the domains we intend to use now for modelling signal analysis. But, of course, we have to generalize them in such a way that a coherent model will emerge. This is most simple in $\mathbb{R}_2$. Besides representing the vector space $\mathbb{R}^2$, there exists an even subalgebra $\mathbb{R}_2^+$ with the basis $\{\mathbf{e}_0,\ \mathbf{e}_{12}\}$. Hence, there is the isomorphism $\mathbb{R}_2^+ \simeq \mathbb{C}$, and I_2 takes on the role of the imaginary unit $j \in \mathbb{C}$. In $\mathbb{R}_3$ the algebra of $\{\mathbf{e}_0,\ \mathbf{e}_{123}\}$ is isomorphic to $\mathbb{C}$. So I_3 takes on the role of the imaginary unit in that subalgebra. Besides, in $\mathbb{R}_3$ and $\mathbb{R}_4$ any even subalgebra over the pair $\{\mathbf{e}_0, B\}$, B being a normalized bivector, is isomorphic to $\mathbb{C}$.

In our approach we want to handle signals f as vectors in the respective GA and mappings of the kind $\mathcal{A} : f \longrightarrow f_A$ of a (multi-dimensional) real signal to a (generalized multi-dimensional) analytic signal as operations of scaling-rotation in the respective GA. We call such operators spinors [34]. A spinor $S \in \mathbb{R}_n^+$ is an even multivector with the norm $S\widetilde{S} = |S|^2$. If $|S|^2 = 1$, then the spinor will be called a rotor [26]. The spinor operation is of fundamental importance for understanding our multi-dimensional phase concept. Therefore, we will give a very short sketch of the ideas of computing with spinors.

A complex number $z \in \mathbb{C}$, $z = x + jy = r\exp(j\theta) = r(\cos\theta + j\sin\theta)$ is replaced in $\mathbb{R}_2^+$ by the multivector $Z = x + yI_2 = r\exp(\theta I_2)$ which rotates $\mathbf{e}_1 \in \mathbb{R}_2$ to $\mathbf{x} = x\mathbf{e}_1 + y\mathbf{e}_2$ by $\mathbf{x} = \mathbf{e}_1 Z$. Because of the non-commutativity of the geometric product in GA, we can also write $\mathbf{x} = \overline{Z}\mathbf{e}_1$ with $\overline{Z}$ being the conjugate of Z, $\overline{Z} = r\exp(-\theta I_2)$. Besides, because of $\exp(\theta I_2) = \left(\exp\left(\frac{\theta}{2}I_2\right)\right)^2$, we will introduce the spinor $S = r\exp\left(\frac{\theta}{2}I_2\right)$ as an element of the spin group Spin(2), see [34], and its conjugate $\overline{S} = r\exp\left(-\frac{\theta}{2}I_2\right)$. Written in terms of that operator, scaling-rotation is given by the spinor product $\mathbf{x} = \overline{S}\mathbf{e}_1 S$ with $S\overline{S} = Z$. Using the spinor representation for scaling-rotation has the advantage of being generalizable to higher dimensions.

A normalized spinor is called a rotor, R. It describes a rotation independent of the dimension of the embedding space. By interpreting a rotation as a Lie group action, in $\mathbb{R}_2$ the pseudoscalar I_2 is the generator of the rotation. The same is with I_3 in $\mathbb{R}_3$. There the rotation plane may be represented by the bivector $B = r_1\mathbf{e}_{23} + r_2\mathbf{e}_{31} + r_3\mathbf{e}_{12}$ which is also $B = \mathbf{r}I_3 = -\mathbf{r}I_3^{-1}$ with $\mathbf{r}$ being the dual of B, the rotation vector. Then, because of $\exp(\mathbf{r}I_3) = \cos|\mathbf{r}| + I_3\frac{\mathbf{r}}{|\mathbf{r}|}\sin|\mathbf{r}|$, $R = \exp\left(\frac{1}{2}\mathbf{r}I_3\right)$ is the rotor describing the rotation of any vector $\mathbf{x} \in \mathbb{R}_3$ to $\mathbf{x}'$ with respect to the axis $\mathbf{r}$ by the angle $|\mathbf{r}|$,

$$\mathbf{x}' = R\mathbf{x}\widetilde{R}, \tag{20}$$

with $\widetilde{R} = \exp\left(-\frac{1}{2}\mathbf{r}I_3\right)$ indicating the reverse of R. With respect to the group Spin(4) in $\mathbb{R}_4$ we advise the reader to [34].

Finally, we want to give an idea of extracting both the amount of a rotation (in classical terms the rotation angle) and its direction in the respective vector space $\mathbb{R}^n$. This is fundamental for extracting both the parity symmetry (the phase angle) and its orientation in space from the phase of the generalized analytic signal. Thinking in terms of signal theory, we can imagine the analytic (or monogenic) signal as the impulse response of a spinor acting on a unit pulse oriented along the respective real axis of the signal model. So the spinor causes a rotation and a scaling of the unit impulse in a complex plane lying in the space $\mathbb{R}^n$. Hence, additional (generalized) imaginary signal components are generated lying in the dual space

of the original real signal within the embedding space of our signal model. The logarithm of the exponential spinor representation gives us access to its generators: scaling corresponds to the local energy and rotation corresponds to the local phase (including orientation in space). Because of our simple model of rotation in a single plane, see [34], the $\mathbb{R}_n^+$-logarithm of a spinor $S \in \mathbb{R}_n^+$ for $n = 2, 3, 4$ in our case reads

$$\log(S) = \log(|S|) + \frac{\langle S \rangle_2}{|\langle S \rangle_2|} \operatorname{atan}\left(\frac{|\langle S \rangle_2|}{\langle S \rangle_0}\right). \tag{21}$$

The scalar part $\langle \log(S) \rangle_0 = \log(|S|)$ corresponds to the logarithm of the local energy and the bivector part of $\log(S)$, $\langle \log(S) \rangle_2 = \arg(S)$, corresponds to the respective phase representation in $\mathbb{R}_n$. While in $\mathbb{R}_2$ this is the well-known phase angle, represented as bivector, in $\mathbb{R}_3$ and $\mathbb{R}_4$ the actual phase indicating parity symmetry is enhanced by one or two orientation angles, respectively.

3.3. **Harmonic Fields in Euclidean Spaces.** Although the term analytic signal immediately should evoke associations to the term analytic function, its relation to the complex analysis is widely unknown in the image processing community. But the understanding of some basic facts of complex analysis will be necessary for extending it to higher dimensional spaces. Our presented approach to parity symmetry estimation in the multi-dimensional case is based on Clifford harmonic analysis [3, 45, 32]. Let n be the dimension of the scalar signal $f(\mathbf{x})$, that is $\mathbf{x} \in \mathbb{R}^n$, $\mathbf{x} = x_1\mathbf{e}_1 + \ldots + x_n\mathbf{e}_n$. We will denote the original signal by $f_n(\mathbf{x})$. Then the embedding dimension of the signal will be $n + 1$. Instead of using the scalar field representation $f_n(\mathbf{x})$, we are considering the analysis of harmonic vector fields $\mathbf{f}_{n+1}(\mathbf{x})$ in GAs $\mathbb{R}_{n+1}$, $n = 1, 2, 3$. In that framework a 2D harmonic field directly corresponds to a 1D analytic function and an $(n+1)$D harmonic field corresponds to an nD monogenic function. Again we restrict ourselves to some necessary key ideas of the derivation of a function theory of $\mathbb{R}_{n+1}$-valued functions derived from harmonic $(n+1)$D vector fields.

Let $\mathbf{g}_{n+1}(\mathbf{x}) = \sum_{i=1}^{n+1} g_{(i)}^{n+1}\mathbf{e}_i$ be a vector field of dimension $n + 1$. Then it is called a harmonic field if it is the gradient field of a harmonic potential $p_{n+1}(\mathbf{x})$, which itself is a scalar field of dimension $n + 1$,

$$\mathbf{g}_{n+1} = \boldsymbol{\nabla}_{n+1} p_{n+1}, \tag{22}$$

with the Dirac operator in $\mathbb{R}_{n+1}$ defined by the vector

$$\boldsymbol{\nabla}_{n+1} = \sum_{i=1}^{n+1} \mathbf{e}_i \frac{\partial}{\partial x_i}. \tag{23}$$

Then the Dirac equation

$$\boldsymbol{\nabla}_{n+1}\mathbf{g}_{n+1} = 0 \tag{24}$$

represents in $\mathbb{R}_{n+1}$ a compact generalized equivalent of the Cauchy-Riemann equations, which are known from complex vector field analysis. But in addition to the Dirac equation, the generalized Cauchy-Riemann equations tell us that also all $n+1$ components $g_{(i)}^{n+1}$ of $\mathbf{g}_{n+1}$ themselves are harmonic. These components constitute an $(n + 1)$-tuple of harmonic conjugates of each other. Splitting the geometric product of equation (24) into its scalar part, $\boldsymbol{\nabla}_{n+1} \cdot \mathbf{g}_{n+1} = 0$, and into its bivector part, $\boldsymbol{\nabla}_{n+1} \wedge \mathbf{g}_{n+1} = 0$, indicates both zero divergence and zero curl of $\mathbf{g}_{n+1}$, respectively, in a generalized sense. Because $\boldsymbol{\nabla}_{n+1} \cdot \mathbf{g}_{n+1} = \boldsymbol{\nabla}_{n+1} \cdot \boldsymbol{\nabla}_{n+1} p_{n+1} =$

$\boldsymbol{\nabla}_{n+1}\boldsymbol{\nabla}_{n+1}p_{n+1} = \Delta_{n+1}p_{n+1}$, zero divergence means that p_{n+1} fulfills the Laplace equation

$$\Delta_{n+1}p_{n+1} = 0, \tag{25}$$

with Δ_{n+1} being the $(n+1)$-dimensional Laplace operator. The fundamental solution of equation (25) takes on different forms in $\mathbb{R}_{n+1}$, $n = 1, 2, 3$:

$$p_2(\mathbf{x}) = \frac{\log\left(|\mathbf{x}|\right)}{\pi}\ ,\ p_3(\mathbf{x}) = -\frac{1}{2\pi|\mathbf{x}|}\ ,\ p_4(\mathbf{x}) = -\frac{1}{4\pi^2|\mathbf{x}|^2}\ , \tag{26}$$

and the respective gradient fields read

$$\mathbf{g}_2(\mathbf{x}) = \frac{\mathbf{x}}{\pi|\mathbf{x}|^2}\ ,\ \mathbf{g}_3(\mathbf{x}) = \frac{\mathbf{x}}{2\pi|\mathbf{x}|^3}\ ,\ \mathbf{g}_4(\mathbf{x}) = \frac{\mathbf{x}}{2\pi^2|\mathbf{x}|^4}. \tag{27}$$

In the equations (26) and (27) and in the following $p_{n+1}(\mathbf{x})$ and $\mathbf{g}_{n+1}(\mathbf{x})$ explicitly indicate scalar or vector valued functions, respectively, defined over $\mathbf{x} \in \mathbb{R}^{n+1}$. While the components $x_1, \ldots, x_n$ of $\mathbf{x}$ are the normal signal coordinates, x_{n+1} will take on a special role as we will see in section 4.2. The components of $\mathbf{g}_2$ form a Hilbert pair and those of $\mathbf{g}_3$ and $\mathbf{g}_4$ form a Riesz triplet and a Riesz quadruple, respectively. Each component can be transformed into the other one by either the Hilbert transform ($n = 1$) or the Riesz transform ($n = 2, 3$) [47].

What remains open is the way to arrive at the analytic signal, respectively the monogenic signal as its generalization, from a (multi-dimensional) real signal. This requires to extend the real function of dimension n in such a way that the resulting function of dimension $n + 1$ fulfills the Cauchy-Riemann equations or the Dirac equation, respectively, in the framework of a vector field model of our signal. This solution can be identified with a harmonic field. The analytic/monogenic completion of a real (multi-dimensional) function $f_n(\mathbf{x})$, n = 1, 2, 3, has its solution in $\mathbb{R}_{n+1}$. It can be derived from the boundary value problem (Dirichlet problem for the upper half-space) [9],[1]

$$\Delta_{n+1}p_{n+1}(\mathbf{x}) \quad = \quad 0 \qquad \text{for } x_{n+1} > 0 \tag{28}$$

and

$$\mathbf{e}_{n+1}\frac{\partial}{\partial x_{n+1}}p_{n+1}(\mathbf{x}) \quad = \quad f_n(\mathbf{x})\mathbf{e}_{n+1} \qquad \text{for } x_{n+1} = 0. \tag{29}$$

The unique solution of these equations results finally in the analytic signal and the monogenic signal, respectively, represented as vector field, $\mathbf{f}_{n+1}(\mathbf{x}) = \boldsymbol{\nabla}_{n+1}p_{n+1}(\mathbf{x})$ for $x_{n+1} > 0$. For $x_{n+1} = 0$ the $\mathbf{e}_{n+1}$-component of $\mathbf{f}_{n+1}(\mathbf{x})$, $f^{n+1}_{(n+1)}(\mathbf{x})$, corresponds to the original signal $f_n(\mathbf{x})$. The other components $f^{n+1}_{(1)}(\mathbf{x}), ..., f^{n+1}_{(n)}(\mathbf{x})$ of $\mathbf{f}_{n+1}(\mathbf{x})$ are the Hilbert/Riesz transformed signal components as part of the analytic/monogenic signal. As we see, the original real signal is directed to the additional coordinate axis $\mathbf{e}_{n+1}$, and the Hilbert/Riesz components are lying in the original space $\mathbb{R}^n$.

4. **2D and 3D Monogenic Signals.** After having summarized the signal theoretic foundations of our problem at hand and after having sketched the algebraic framework we use for embedding our signals, we will now present the solutions more in detail as indicated in section 3.3. This makes necessary to first specify our signal model and to comment the handling of operators and filters, both in spatial and frequency domain. After that we will derive the monogenic signals and discuss their respective local spectral representations. Of special interest, of course, will be the

gained phase concept. Finally, we will shortly discuss the new scale-space that is intrinsic to the presented solution.

4.1. **Basics of Signal Theory in Geometric Algebras.** As mentioned in section 3.3, we are using a vector field representation, $\mathbf{f}_{n+1}(\mathbf{x})$, of our real signals $f_n(\mathbf{x})$, $n = 1, 2, 3$, to get the analytic signal $\mathbf{f}_A(\mathbf{x})$, $\mathbf{x} \in \mathbb{R}^2$ and the monogenic signals $\mathbf{f}_M(\mathbf{x})$, $\mathbf{x} \in \mathbb{R}^3$ or $\mathbf{x} \in \mathbb{R}^4$, respectively. The vector field of the original signal in $\mathbb{R}_{n+1}$ in our chosen embedding for $x_{n+1} = 0$ reads

$$\mathbf{f}_{n+1}(\mathbf{x}) = \mathbf{f}_{n+1}(x_1\mathbf{e}_1 + \ldots + x_{n+1}\mathbf{e}_{n+1}) = f_n(x_1, ..., x_n)\mathbf{e}_{n+1}, \tag{30}$$

The Fourier transform of a general multivector valued function $g_{n+1}(\mathbf{x})$, $\mathbf{x} \in \mathbb{R}^{n+1}$, in $\mathbb{R}_{n+1}$ is given by

$$G_{n+1}(\mathbf{u}) = \mathcal{F}_n \left\{ g_{n+1}(\mathbf{x}) \right\} (\mathbf{u}), \tag{31}$$

where $\mathcal{F}_n$ means that the Fourier transform is only performed with respect to the original signal coordinates $x_1, ..., x_n$. The imaginary unit is replaced by I_2 in the 1D case and by I_3 in the 2D case. In the 3D case also I_3 is used because I_4 does not square to minus one. This special choice of the Fourier transform is adapted to our models of signals and operators. For a more general Fourier transform on multivector valued functions with application in image processing see [12]. What we also need is that all bivectors of $\mathbb{R}_3$ and $\mathbb{R}_4$ square to minus one and, thus, enable access to the complex domain rotating in the embedding space. The Fourier transform is isotropic in each case, but its effect looks different in dependence of the function g.

A signal representation $\mathbf{f}_{n+1}(\mathbf{x}) = f^{n+1}_{(1)}(\mathbf{x})\mathbf{e}_1 + ... + f^{n+1}_{(n+1)}(\mathbf{x})\mathbf{e}_{n+1}$ in $\mathbb{R}_{n+1}$, $n = 1, 2, 3$, transforms according to

$$\mathbf{F}_{n+1}(\mathbf{u}) = \mathcal{F}_n \left\{ \mathbf{f}_{n+1}(\mathbf{x}) \right\} (\mathbf{u}) = F^{n+1}_{(1)}(\mathbf{u})\mathbf{e}_1 + ... + F^{n+1}_{(n+1)}(\mathbf{u})\mathbf{e}_{n+1} \tag{32}$$

with $F^{n+1}_{(i)} = F^{n+1,e}_{(i)} + F^{n+1,o}_{(i)} I_{n+1}$ for $n = 1, 2$ and $i = 1, \ldots, n+1$. This indicates an advantage of using a vector valued signal representation in comparison to the classic approach in multiple dimensions: each component of the signal is transformed separately. In the 3D case we get

$$\begin{aligned} \mathbf{F}_4(\mathbf{u}) &= F^{4,e}_{(1)}(\mathbf{u})\mathbf{e}_1 + F^{4,o}_{(1)}(\mathbf{u})\mathbf{e}_{23} + F^{4,e}_{(2)}(\mathbf{u})\mathbf{e}_2 + F^{4,o}_{(2)}(\mathbf{u})\mathbf{e}_{31} \\ &+ F^{4,e}_{(3)}(\mathbf{u})\mathbf{e}_3 + F^{4,o}_{(3)}(\mathbf{u})\mathbf{e}_{12} + F^{4,e}_{(4)}(\mathbf{u})\mathbf{e}_4 + F^{4,o}_{(4)}(\mathbf{u})I_3. \end{aligned} \tag{33}$$

Filter kernels, $h(\mathbf{x})$, are supposed to be spinor valued to map a vector valued signal to a vector valued signal by convolution. But instead of applying the exponential form of a spinor and designing a convolution based on the sandwich form of the spinor product, see equation (20), a left hand convolution theorem reads $\mathcal{F}_n \left\{ (h * f)(x) \right\} (\mathbf{u}) = H(\mathbf{u})\mathbf{F}(\mathbf{u})$ with $\mathbf{x}, \mathbf{u} \in \mathbb{R}^n$. Just as the vector valued signal, a spinor h transforms component-wise but with another symmetry, $H(-\mathbf{u}) = H(\mathbf{u})$, e.g. for $n = 2$:

$$\begin{aligned} H_3(\mathbf{u}) &= \mathcal{F}_2 \left\{ h_3(\mathbf{x}) \right\} (\mathbf{u}) \\ &= H_0(\mathbf{u}) + H_{23}(\mathbf{u})\mathbf{e}_{23} + H_{31}(\mathbf{u})\mathbf{e}_{31} + H_{12}(\mathbf{u})\mathbf{e}_{12}. \end{aligned} \tag{34}$$

Hence, the frequency response of a spinor is spinor valued again. The same is with that one of a scalar. The Fourier transform of a scalar potential field, $p(\mathbf{x})$, as a special case of a spinor, is given for $n = 1, 2$ by

$$P_{n+1}(\mathbf{u}) = \mathcal{F}_n \left\{ p_{n+1}(\mathbf{x}) \right\} (\mathbf{u}) = P^e_{n+1}(\mathbf{u}) + P^o_{n+1}(\mathbf{u})I_{n+1} \tag{35}$$

and for $n = 3$ by $P_4(\mathbf{u}) = \mathcal{F}_3\left\{p_4(\mathbf{x})\right\}(\mathbf{u}) = P_4^e(\mathbf{u}) + P_4^o(\mathbf{u})I_3$.

The most important operator, which is not a filter in the above mentioned sense in our embedding scheme, is the derivative operator (Dirac operator) $\boldsymbol{\nabla}_{n+1} = \sum_{i=1}^{n+1} \mathbf{e}_i \frac{\partial}{\partial x_i}$. It is a vector which, nevertheless, can be reformulated as a filter by multiplication with a vector valued Dirac delta function. The Fourier transform of its action to a vector valued function $\mathbf{g}_{n+1}(\mathbf{x})$ in $\mathbb{R}_{n+1}$ reads for

$$\begin{array}{lll} n=1: & \mathcal{F}_1\left\{\boldsymbol{\nabla}_2\mathbf{g}_2(\mathbf{x})\right\}(\mathbf{u}) & = 2\pi\mathbf{u}I_2G_2(\mathbf{u}) \\ n=2: & \mathcal{F}_2\left\{\boldsymbol{\nabla}_3\mathbf{g}_3(\mathbf{x})\right\}(\mathbf{u}) & = 2\pi\mathbf{u}I_3G_3(\mathbf{u}) \\ n=3: & \mathcal{F}_3\left\{\boldsymbol{\nabla}_4\mathbf{g}_4(\mathbf{x})\right\}(\mathbf{u}) & = 2\pi\mathbf{u}I_3G_4(\mathbf{u}). \end{array} \tag{36}$$

The second derivative is given by the Laplace operator Δ_{n+1} with its Fourier transform $\mathcal{F}_n\left\{\Delta_{n+1}(\mathbf{x})\right\}(\mathbf{u}) = -4\pi^2\mathbf{u}^2$ independent of n.

4.2. **Poisson Kernel and Riesz Transform.** Now we will have a closer look on the fundamental solutions, equations (26), of the Laplace equation (25), respectively on the gradient fields, equations (27), for signals embedded according to equation (30). First, we consider the $\mathbf{e}_{n+1}$-component, $f_{(n+1)}^{n+1}(\mathbf{x})$, of $\mathbf{f}_{n+1}(\mathbf{x})$, $\mathbf{x} \in \mathbb{R}^{n+1}$. According to equation (30) this component corresponds to the original real signal $f_n(\mathbf{x})$ for $x_{n+1} = 0$. Next, we are interested in the changes happening in the half space $x_{n+1} > 0$. The $\mathbf{e}_{n+1}$-component for that case will be obtained from the x_{n+1}-derivative of $p_{n+1}(\mathbf{x})\mathbf{e}_{n+1}$. This results in the scalar function

$$f_{(n+1)}^{n+1}(\mathbf{x}) = (\mathbf{f}_{n+1} \cdot \mathbf{e}_{n+1})(\mathbf{x}) = \mathbf{e}_{n+1}\frac{\partial}{\partial x_{n+1}} p_{n+1}(\mathbf{x})\mathbf{e}_{n+1}, \tag{37}$$

which for $\mathbf{x} \in \mathbb{R}^n$ reads

$$l_{n+1}(\mathbf{x}, x_{n+1}) = (\mathbf{f}_{n+1} \cdot \mathbf{e}_{n+1})(\mathbf{x}, x_{n+1}) = \frac{a_n x_{n+1}}{|\mathbf{x} + x_{n+1}\mathbf{e}_{n+1}|^{n+1}} \tag{38}$$

with $a_n = \pi^{-\frac{n+1}{2}}\Gamma\left(\frac{n+1}{2}\right)$.

This scalar valued function is the nD Poisson kernel [47, 45]. A convolution of the original signal, embedded into $\mathbb{R}^{n+1}$ according to $\mathbf{f}_{n+1}^0(\mathbf{x}) = \mathbf{f}(x_1\mathbf{e}_1 + \ldots + x_n\mathbf{e}_n)\delta_0(x_{n+1})$, with the Poisson kernel results in the signal representation $\mathbf{f}_{n+1}^l(\mathbf{x})$ for any chosen $x_{n+1} > 0$, see [1],

$$\mathbf{f}_{n+1}^l(\mathbf{x}, x_{n+1}) = \left(l_{n+1} * \mathbf{f}_{n+1}^0\right)(\mathbf{x}, x_{n+1}), \qquad \mathbf{x} \in \mathbb{R}^n. \tag{39}$$

Here x_{n+1} takes on the role of a parameter. The effect of that convolution can be seen best in the frequency domain. Because the choice of $\mathbf{f}_{n+1}^0$ leads to an absorption of the convolution over the x_{n+1}-coordinate, we get

$$\mathbf{F}_{n+1}^l(\mathbf{u}, x_{n+1}) = \mathcal{F}\left\{\mathbf{f}_{n+1}^l\right\}(\mathbf{u}, x_{n+1}) = L_{n+1}(\mathbf{u}, x_{n+1})\mathbf{F}_{n+1}^0(\mathbf{u}) \tag{40}$$

with $\mathbf{u} \in \mathbb{R}^n$. The Fourier transform of the Poisson kernel,

$$L_{n+1}(\mathbf{u}, x_{n+1}) = \exp\left(-2\pi|\mathbf{u}|x_{n+1}\right), \tag{41}$$

indicates a lowpass characteristic, which is parameterized by the augmented coordinate x_{n+1} of our chosen embedding. Hence, x_{n+1} has to be interpreted as a scale parameter and the vector $\mathbf{x} \in \mathbb{R}^{n+1}$ spans a linear scale-space, the Poisson scale-space [20], whose generating blurring operator is the Poisson kernel. We will come back to that point in section 4.4.

Now we will enlighten the components $f_{(1)}^{n+1}(\mathbf{x}), \ldots, f_{(n)}^{n+1}(\mathbf{x})$ of $\mathbf{f}_{n+1}(\mathbf{x})$, $\mathbf{x} \in \mathbb{R}^{n+1}$, in the half space $x_{n+1} > 0$. They constitute the bivector

$$(\mathbf{f}_{n+1} \wedge \mathbf{e}_{n+1})(\mathbf{x}) = \sum_{i=1}^{n} \mathbf{e}_i \frac{\partial}{\partial x_i} p_{n+1}(\mathbf{x}) \mathbf{e}_{n+1}. \tag{42}$$

For $\mathbf{x} \in \mathbb{R}^n$ this bivector in $\mathbb{R}_{n+1}$ reads

$$h_{n+1}(\mathbf{x}, x_{n+1}) = (\mathbf{f}_{n+1} \wedge \mathbf{e}_{n+1})(\mathbf{x}, x_{n+1}) = \frac{a_n \mathbf{x} \mathbf{e}_{n+1}}{|\mathbf{x} + x_{n+1}\mathbf{e}_{n+1}|^{n+1}}. \tag{43}$$

This function is the conjugate Poisson kernel [45]. It represents a compound operator, which again best can be seen in the Fourier domain with $\mathbf{u} \in \mathbb{R}^n$,

$$\begin{aligned} H_{n+1}(\mathbf{u}, x_{n+1}) &= \mathcal{F}\left\{h_{n+1}(\mathbf{x}, x_{n+1})\right\}(\mathbf{u}, x_{n+1}) \\ &= \frac{\mathbf{u}}{|\mathbf{u}|} I_{n+1}^{-1} \exp\left(-2\pi|\mathbf{u}|x_{n+1}\right), \end{aligned} \tag{44}$$

or

$$H_{n+1}(\mathbf{u}, x_{n+1}) = R_n(\mathbf{u}) L_{n+1}(\mathbf{u}, x_{n+1}), \tag{45}$$

respectively. While L_{n+1} is known from equation (41) to be the Poisson kernel, $R_n(\mathbf{u})$ is the Riesz transform in Fourier representation. The Riesz transform [47] is the formerly mentioned generalization of the Hilbert transform with respect to the dimension. It coincides with the Hilbert transform for $n = 1$. Its definition in $\mathbb{R}_{n+1}$ for $\mathbf{x}$, $\mathbf{u} \in \mathbb{R}^n$ is given by the bivector

$$r_n(\mathbf{x}) = \frac{a_n \mathbf{x} \mathbf{e}_{n+1}}{|\mathbf{x}|^{n+1}}, \tag{46}$$

and

$$R_n(\mathbf{u}) = \frac{\mathbf{u}}{|\mathbf{u}|} I_{n+1}^{-1}, \tag{47}$$

respectively. This isotropic operator is identical with the first order nD spherical harmonic.

The analytic signal as well as the Hilbert transform are well known to practitioners in signal processing. However, their multi-dimensional generalizations to the monogenic signal and the Riesz transform were not known so far. Only in year 2000 some researchers simultaneously came to the solution for $n = 2$, see [13] for references. For $n = 3$ we presented the first application in image sequence analysis in [30]. Quite other is the situation in mathematics in the field of Calderon-Zygmund theory [8, 46], where also relations to the wavelet theory have been established [35]. Completely unknown was so far the relation of this signal modelling to the linear scale-space theory until the paper [17] and the report [18]. There is a difference in the representation of the Hilbert transform between the one which results for $n = 1$ from equations (46) or (47) and the one in equation (3), which is normally used in signal processing. While r_1 subsumes the imaginary unit as $j \equiv \mathbf{e}_{12}$, $h(x)$ in equation (3) is real and scalar valued. Equation (46) establishes an n-dimensional $\mathbb{R}_{n+1}$-valued monogenic completion of an n-dimensional real valued signal. The understanding of the relations between the Riesz transform for multi-dimensional signals and the Hilbert transform for 1D signals may also be supported by remembering the well-known Radon transform, see e.g. [41]. As discussed more in detail in [16, 13] for $n = 2$, from the Fourier slice theorem follows that the Riesz transform may be interpreted as the linear superposition of the oriented Hilbert transforms

of the intrinsically 1D signal components. But embedding the n-dimensional signal into $\mathbb{R}_{n+1}$ according to $x_{n+1} > 0$ additionally generalizes this concept by the emergence of the Poisson kernel. According to equation (45), a smoothed Riesz transformed signal representation may be computed by either convolving the original signal with the conjugate Poisson kernel, by convolving first with the Poisson kernel, followed by the Riesz transform or by concatenating both operators in the reverse order. These relations follow from the fact that all involved transforms are linear ones.

4.3. **Monogenic Signal and Phase in nD Case.** Now we will discuss more in detail the monogenic signal, $\mathbf{f}_M(\mathbf{x})$, as the generalized analytic signal, $\mathbf{f}_A(\mathbf{x})$, which corresponds to our vector field $\mathbf{f}_{n+1}(\mathbf{x})$ in the last section. In this section we restrict ourselves to the case $x_{n+1} = 0$, but we will sketch the case $x_{n+1} > 0$ in the next section.

The monogenic signal is defined in $\mathbb{R}_{n+1}$ by

$$\mathbf{f}_M(\mathbf{x}) = \mathbf{f}(\mathbf{x}) + \mathbf{f}^r(\mathbf{x}) = \mathbf{f}(\mathbf{x}) + (r_n * \mathbf{f})(\mathbf{x}), \tag{48}$$

respectively

$$\mathbf{f}_M(\mathbf{x}) = f_n(\mathbf{x})\mathbf{e}_{n+1} + f^r_{(1)}(\mathbf{x})\mathbf{e}_1 + \ldots + f^r_{(n)}(\mathbf{x})\mathbf{e}_n. \tag{49}$$

The monogenic signal can be interpreted as the action of a spinor $S(\mathbf{x}) = \mathbf{e}_{n+1}\mathbf{f}_M(\mathbf{x})$ which transforms a unit impulse $\mathbf{e}_{n+1}$ to $\mathbf{f}_M(\mathbf{x})$. Remembering equation (21), both local amplitude

$$a(\mathbf{x}) = |\mathbf{f}_M(\mathbf{x})| = \exp\left(\langle \log\left(\mathbf{e}_{n+1}\mathbf{f}_M(\mathbf{x})\right)\rangle_0\right) \tag{50}$$

and generalized local phase, that is the Riesz phase,

$$\Phi_n(\mathbf{x}) = \arg\left(\mathbf{f}_M(\mathbf{x})\right) = \langle \log\left(\mathbf{e}_{n+1}\mathbf{f}_M(\mathbf{x})\right)\rangle_2 \tag{51}$$

can be computed. These local spectral representations suggest a spherical representation of the monogenic signal,

$$f_M(\mathbf{x}) = a(\mathbf{x}) \exp\left(\Phi_n(\mathbf{x})\right), \tag{52}$$

which is now $\mathbb{R}^+_{n+1}$-valued.

Most interesting is the study of the Riesz phase bivector $\Phi_n(\mathbf{x})$ because this will enable us to get access to the local symmetry in the multi-dimensional case. An intuitive interpretation of the Riesz phase in the nD case can be found by maintaining the model of the 1D phase, embedded into $\langle\mathbb{R}_{n+1}\rangle_1$. There exists a phase plane $\mathbf{f}_M(\mathbf{x}) \wedge \mathbf{e}_{n+1} = \langle \mathbf{e}_{n+1}\mathbf{f}_M(\mathbf{x})\rangle_2$, which corresponds to the complex plane known from 1D. Within that plane the phase angle $\varphi(\mathbf{x})$ describes the rotation caused by the Riesz transform, respectively by the Hilbert transform. In nD, $n > 1$, there are additional orientation angles $\{\theta_1, \ldots, \theta_{n-1}\}$, which determine the orientation of the phase plane within $\langle\mathbb{R}_{n+1}\rangle_1$.

Figure 1 visualizes that model. As we see, the parity symmetry analysis is strongly coupled to the orientation analysis of an i1D structure embedded into $\mathbb{R}^n$. The orientation angles are in the spatial domain. For $n = 2$ the even and odd parity symmetries are shown in addition.

To formalize the existence of these components of $\Phi_n(\mathbf{x})$, we will have a closer look on equation (51). We can write

$$\Phi_n(\mathbf{x}) = \frac{\langle \mathbf{e}_{n+1}\mathbf{f}_M(\mathbf{x})\rangle_2}{|\langle \mathbf{e}_{n+1}\mathbf{f}_M(\mathbf{x})\rangle_2|} \operatorname{atan}\left(\frac{|\langle \mathbf{e}_{n+1}\mathbf{f}_M(\mathbf{x})\rangle_2|}{|\langle \mathbf{e}_{n+1}\mathbf{f}_M(\mathbf{x})\rangle_0|}\right). \tag{53}$$

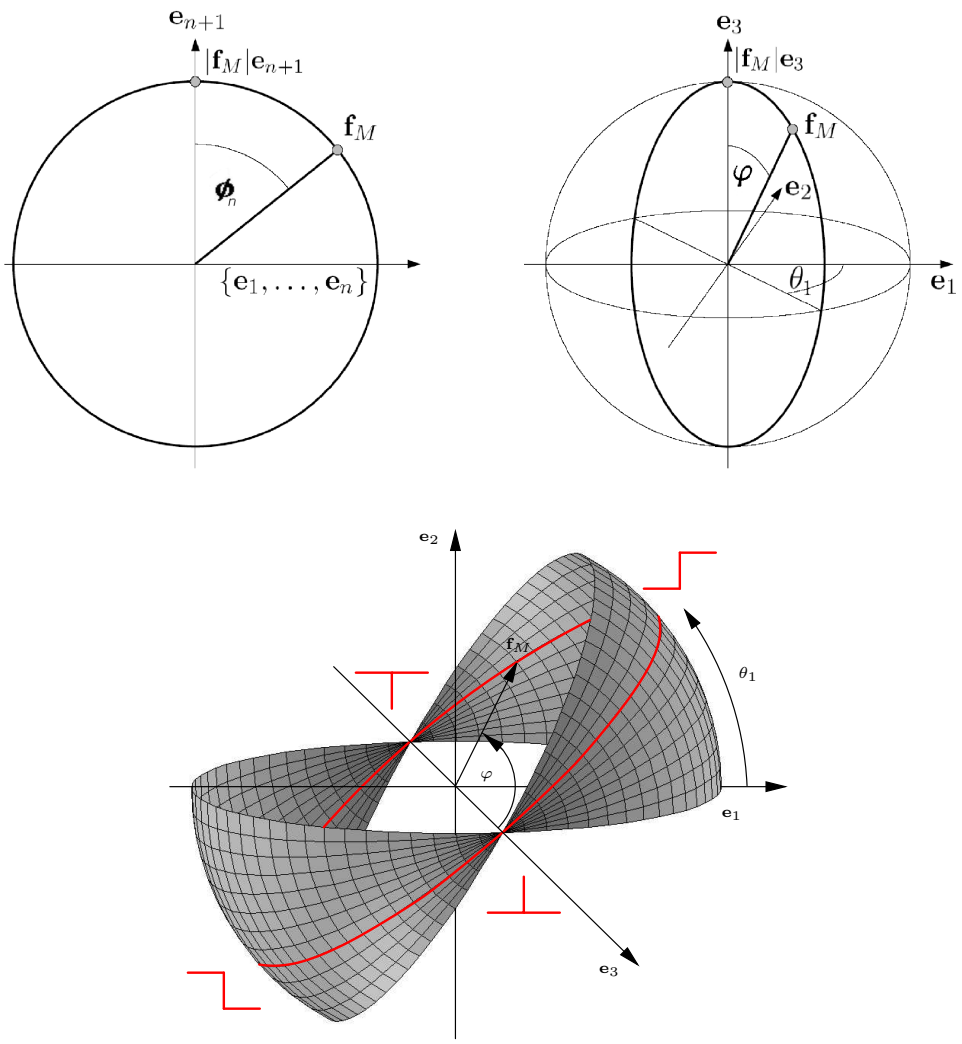

FIGURE 1. The figure shows top left the embedding of the monogenic signal in $\mathbb{R}^{n+1}$. Top right, the special case $n = 2$ is visualized. Bottom: For $n = 2$, parity symmetries are shown in addition.

Obviously, the expression of the arc tangent describes the local phase $\varphi(\mathbf{x})$ as the relation of the magnitudes of the bivector coded Riesz component $\mathbf{f}^r(\mathbf{x})$ and the original real valued component $\mathbf{f}(\mathbf{x})$ of the monogenic signal according to equation (48). This rotation happens in the phase plane $\mathbf{f}_M \wedge \mathbf{e}_{n+1}$, whose orientation in $\mathbb{R}^{n+1}$ is given by the normalized bivector factor of $\Phi_n(\mathbf{x})$. Because $\langle \mathbf{e}_{n+1}\mathbf{f}_M(\mathbf{x})\rangle_2 = \mathbf{e}_{n+1}\mathbf{f}^r(\mathbf{x})$, by means of the inner product

$$\frac{\langle \mathbf{e}_{n+1}\mathbf{f}_M(\mathbf{x})\rangle_2 \cdot \mathbf{e}_{n+1}}{|\langle \mathbf{e}_{n+1}\mathbf{f}_M(\mathbf{x})\rangle_2|} = \frac{\mathbf{f}^r(\mathbf{x})}{|\mathbf{f}^r(\mathbf{x})|}, \tag{54}$$

we get the normalized Riesz component of the monogenic signal as a vector representation of the orientation. This projection from $\mathbb{R}_{n+1}$ to $\mathbb{R}^n$ is reasonable because orientation is a geometric feature of $\mathbb{R}^n$. In fact, there are diverse other ways of

decomposing the nD phase $\Phi_n(\mathbf{x})$. In [13] a rotation vector representation has been used for $n = 2$. But this is not applicable in the case $n = 3$.

In figure 2, the rotation invariance of the amplitude and phase response in the case of a 3D isotropic signal is demonstrated. The pattern has both even and odd symmetry. This can be identified in the phase image. These two symmetry contributions to the amplitude are separately visualized in the two figures at the bottom. See also [30] for an application of the 3D monogenic signal in phase based motion estimation.

To summarize the result of this section we can state that the chosen nD signal model enables a rich local characterization of i1D structures. In a rotation invariant way three orthogonal local features can be derived. These are the local amplitude as measure of the signal energy, the local phase as structural feature describing the parity symmetry, and the local orientation as geometric feature. The last one is delivered for free without any steering. This multiplet of features forms again a harmonic vector field.

4.4. **Monogenic Scale-Space and Spherical Quadrature Filters.** While in the last section we discussed the case $x_{n+1} = 0$ for our augmented signal representation in $\mathbb{R}_{n+1}$, we will sketch in this section the monogenic completion of a multi-dimensional signal in the half-space $x_{n+1} > 0$. Because we already identified x_{n+1} in section 4.2 as a scale parameter, we will set now $s \equiv x_{n+1}$ as scale.

The general signal model of the preceding sections extends the analytic signal in a natural way to the monogenic signal by the solution of the Laplace equation (25). If we consider the coupling of that signal model to a scale, several linear scale-space models will be established. These models are interesting alternatives to the Gaussian scale-space which results from the heat equation [33]. In contrast to a Gaussian scale-space theory not only the intensity of the signal and its gradient can be considered as features of the scaled signal. Instead, local amplitude, phase and orientation become scale-dependent features, which constitute simultaneously a Riesz multiplet.

We have to distinguish between the Poisson scale-space, the analytic, and the monogenic scale-space in dependence on applying either the Poisson kernel, equation (38), or the conjugate Poisson kernel, equation (43), see [20]. The Poisson scale-space and its harmonic conjugate form the analytic/monogenic scale-space. In the analytic/monogenic scale-space the figure flow and the original signal are in quadrature phase relation at each scale.

To take advantage of that, the expressions for the local amplitude and the local phase, equations (50) and (51) have to be generalized accordingly. Let

$$\mathbf{f}_M^s(\mathbf{x}, s) = \mathbf{f}_s(\mathbf{x}, s) + \mathbf{f}_s^r(\mathbf{x}, s) \tag{55}$$

be the monogenic signal at scale s with $\mathbf{x} \in \mathbb{R}^n$. Then, the logarithm of the local amplitude, that is the local attenuation, in the monogenic scale-space reads

$$A(\mathbf{x}, s) = \frac{1}{2} \log \left(|\mathbf{f}_s(\mathbf{x}, s)|^2 + |\mathbf{f}_s^r(\mathbf{x}, s)|^2 \right). \tag{56}$$

The attenuation is introduced instead of the amplitude, because in 1D according to [37] the local attenuation and the phase response of a minimum phase filter form a Hilbert pair. In [20] it is shown that this relation under certain conditions can be extended to nD if i1D signals are considered in the half-plane $s > 0$. Then, the local attenuation $A(\mathbf{x}, s)$ and the Riesz phase $\Phi_n(\mathbf{x}, s)$ constitute a Riesz multiplet,

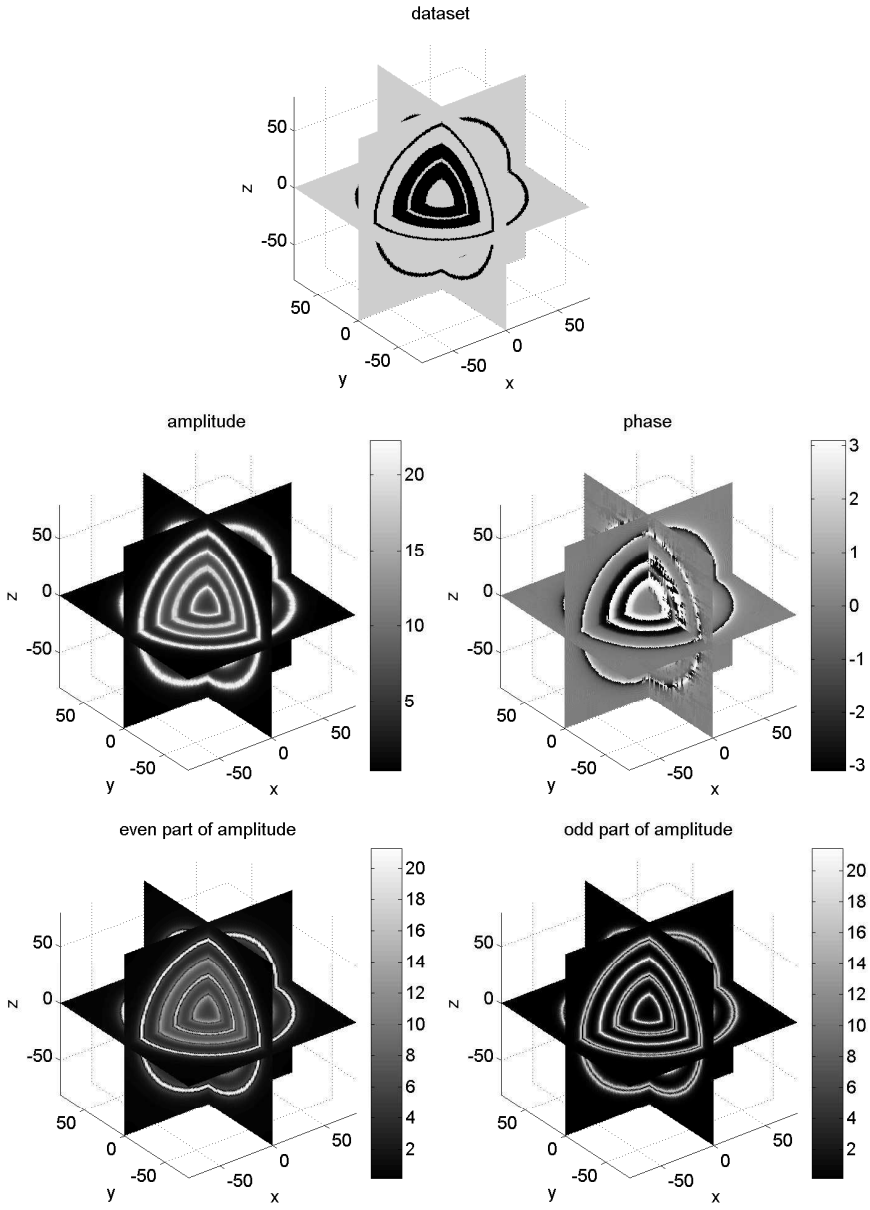

FIGURE 2. The isotropy properties of the monogenic signal in 3D. Top: Cubic image containing concentric spheres. Middle left: Amplitude of the monogenic signal. Middle right: Monogenic phase. There is a phase wrapping taking place in the plane $x = 0$. Bottom: Even and odd parts of the amplitude of the monogenic signal.

that is

$$\Phi_n(\mathbf{x}, s) \approx (r_n * A)(\mathbf{x}, s). \tag{57}$$

The Riesz phase in the monogenic scale-space is given by

$$\Phi_n(\mathbf{x}, s) = \frac{\mathbf{f}_s^r(\mathbf{x}, s)}{|\mathbf{f}_s^r(\mathbf{x}, s)|} \operatorname{atan}\left(\frac{|\mathbf{f}_s^r(\mathbf{x}, s)|}{|\mathbf{f}_s(\mathbf{x}, s)|}\right). \tag{58}$$

In [20] several features of these new scale-space representations are analyzed. Additionally, there is a discussion of the reasons why in contrast to the statement of Iijima [29] besides the Gaussian scale-space also other linear scale spaces should exist. Interestingly, in [11] the authors come to similar conclusions because of quite other reasons. Both studies, [20] and [11], are in accordance with another paper [38]. There the authors propose the so-called α-scale-spaces, generated by smoothing kernels with some properties, where $\alpha = 0$ corresponds to the identity operator, $\alpha = 0.5$ corresponds to the Poisson kernel and $\alpha = 1$ corresponds to the Gaussian kernel, see also [10]. Interestingly, in [40] the authors show how Poisson and Gaussian kernels are deducible from certain powers of the Laplacian applied to harmonic functions without concluding their potential of generating scale-spaces.

An efficient implementation of the monogenic scale-space based on the cosine transform can be found in [15]. The design of isotropic quadrature filters as bandpass filters with quadrature phase relations between the components of the multiplets is another important topic, e.g. for performing a multi-resolution analysis. The most simple approach is to apply both the Poisson kernel and the conjugate Poisson kernel at two different scales, say a coarse scale c and a fine scale f with $c > f$ and $f > 0$. Then a bandpass filtered monogenic signal results,

$$\begin{aligned} \mathbf{f}_M^{c,f}(\mathbf{x}, s) &= \mathbf{f}_M^s(\mathbf{x}, c) - \mathbf{f}_M^s(\mathbf{x}, f) \\ &= (l_{ss} * \mathbf{f})(\mathbf{x}, c, f) + (h_{ss} * \mathbf{f})(\mathbf{x}, c, f) \end{aligned} \tag{59}$$

with the Difference-of-Poisson kernel (DOP) l_{ss} and the Difference-of-conjugate-Poisson kernel (DOCP) h_{ss},

$$l_{ss}(\mathbf{x}, c, f) = l_s(\mathbf{x}, c) - l_s(\mathbf{x}, f) \tag{60}$$

$$h_{ss}(\mathbf{x}, c, f) = h_s(\mathbf{x}, c) - h_s(\mathbf{x}, f). \tag{61}$$

Figure 3 shows the application of these DOP and DOCP filters for the phase based reconstruction of an image in the monogenic scale-space [49]. The problem at hand is that phase based image reconstruction based on Gabor filters uses only a coarse orientation sampling. In the monogenic scale-space instead, the orientation adapts automatically to the structure at each scale. So the reconstruction with that approach outperforms the classical one in the complex domain.

In [14] there is a slightly other approach to design two-dimensional polar separable bandpass filters. There the z-transform is used to compute the coefficients of a series of Poisson filters and the coupling with spherical harmonics of higher order is applied for getting arbitrary radial and azimuthal passbands.

4.5. **Extensions to the Intrinsically 2D Case.** So far we studied the embedding of i1D structures in global nD signals with respect to their local analysis of the phase and thus, of the parity symmetry. In natural images a local patch may be to a certain degree of intrinsic dimension one and to another degree of another intrinsic dimension. And this will change in dependence of the scale.

There is no general way to completely specify the symmetry of an arbitrary i2D structure by applying a pre-designed general operator as in the case of i1D structures. But it should be possible to use the algebraic principles which we described in the preceding sections for coping with special cases of i2D structures. Hopefully,

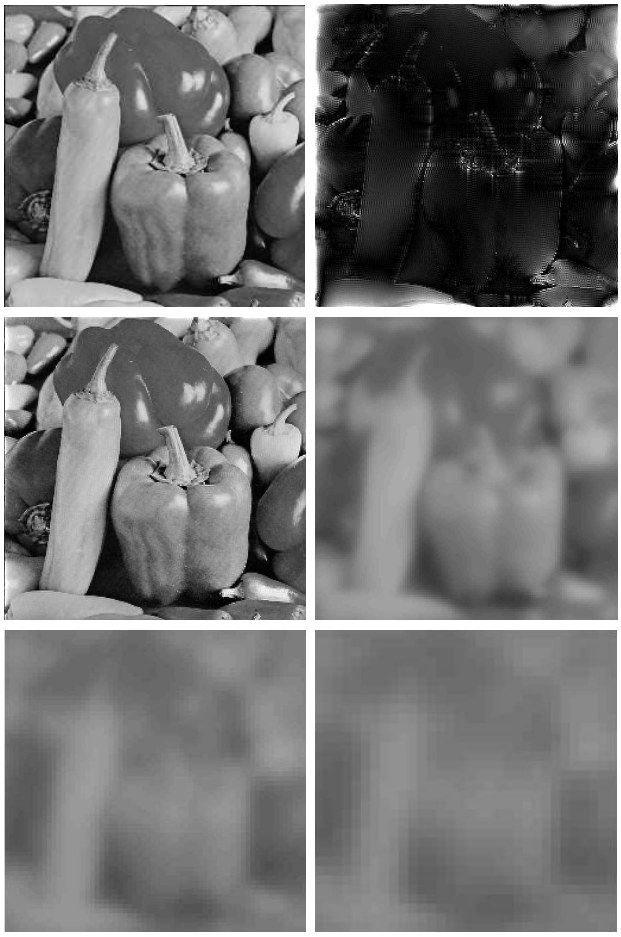

FIGURE 3. Image reconstruction in the monogenic scale-space. Top row: The original image and the absolute error image (the error measure is multiplied by a factor of ten for visualization purpose). Middle row: The left image indicates the final reconstruction (the normalized mean square error (NMSE) is 0.0026). Bottom row and middle row right: The three intermediate reconstructions are zoomed in at the same size of the final reconstruction.

by doing that, we learn more about the nature of i2D signals, so that we will be able in future to analyse also their structures with linear methods. Contemporary mostly non-linear approaches are applied for the analysis of i2D structures.

Our first attempt of the design of a specific operator is called structure multivector [19]. The underlying structure model consists of two perpendicularly crossing i1D structures of arbitrary symmetry. We designed a special set of operators based on the principles of the monogenic signal. But to cope with the involved symmetry combinations, we used complex harmonics of order zero to three instead of only order one as in the case of the monogenic signal. Let $g_s^{(k)}(\mathbf{x})$ be the 2D impulse response of a spherical harmonic filter of order k with $g_s^{(0)}(\mathbf{x}) \equiv \delta(\mathbf{x})$ and

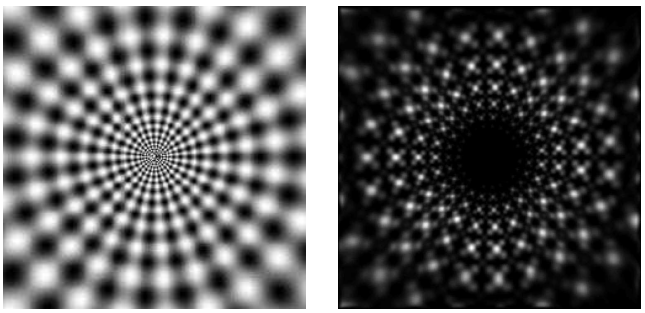

FIGURE 4. Left: Star-like i2D pattern. Right: Amplitude image. The amplitude output illustrates the rotation invariance property of the operator.

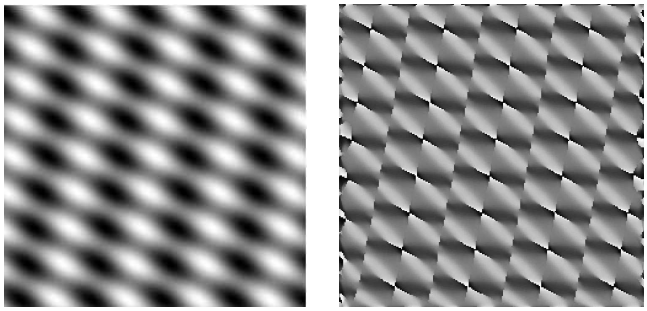

FIGURE 5. Left: The original image as superposition of two cosine signals with different frequencies, amplitudes and orientations. Right: Evaluated phase information.

$g_s^{(1)}(\mathbf{x}) \equiv r_2(\mathbf{x})$. Then

$$S(\mathbf{x}) = \sum_{k=0}^{3} (g_s^{(k)} * \mathbf{f})(\mathbf{x}) \tag{62}$$

enables in $\mathbb{R}_3$ a mapping of the local structure to a 7-dimensional multivector,

$$S = s_0 + s_1\mathbf{e}_1 + s_2\mathbf{e}_2 + s_3\mathbf{e}_3 + s_{23}\mathbf{e}_{23} + s_{31}\mathbf{e}_{31} + s_{12}\mathbf{e}_{12}, \tag{63}$$

called structure multivector. Obviously, equation (62) represents a generalization of the monogenic signal with respect to an i2D structure. Hence, a split of identity of any 2D signal, projected to the model, can be realized in the scale-space. There are five independent features derived from the structure multivector. These are the local (main) orientation, two local i1D amplitudes and two local i1D phases. A major amplitude and a minor amplitude and their respective phases are distinguished. The occurrence of a minor amplitude indicates the i2D nature of the local pattern. For details the reader is referred to [13, 19].

The filter can be used to recognize both i1D and i2D structures, but in contrast to other filters, which respond either to i1D or to i2D structure or mix the responses in an unspecific manner, this filter is simultaneously specific to each type of structure. Regrettably, the evaluation of the structure multivector needs some steering of

orientation. Besides, the involved model of perpendicularly crossing i1D structures is too rigid.

In a second approach another way is gone to compute the split of identity with respect to a more flexible model, where the enclosed angle between two crossing i1D structures is variable [50]. Interestingly, the model subsumes the monogenic signal as special case. In the following, we will give a short sketch of the method. More details can be found in [52].

The monogenic signal is derived from the monogenic extension of a scalar field. Its restriction to i1D functions, embedded in nD signals, results from taking only a minimum of information into account, that is the scalar value $f(\mathbf{x})$. But, if we interpret images as surfaces in $\mathbb{R}^3$, the first and second fundamental theorems of differential geometry would deliver the most general local signal model in the classical framework. Contemporary we neglect the metric tensor, but concentrate on the curvature tensor. If we associate a curvature tensor instead of a scalar value to a location of interest, it is well known that from the mean and the Gaussian curvature a complete classification of the local structure into the types i2D (elliptic and hyperbolic), i1D (parabolic) and i0D (planar) in principle can be done.

Our proposal is to embed the entries of the curvature tensor, which in our work is represented as the Hessian matrix, into $\mathbb{R}_3$. The Hessian matrix results from applying a Hessian derivative operator matrix to an image. The components of this operator matrix are modelled as even harmonic functions of order zero and two. This even matrix is monogenically completed by an odd one as the conjugate of the Hessian operator which consists of spherical harmonics of order one and three. These tensor valued operators, applied to the image function, result in a pair of harmonic conjugate signal representations, called even and odd curvature tensors, T_e and T_o, respectively of the signal. Both together are represented by the monogenic curvature tensor $T(\mathbf{x}) = T_e(\mathbf{x}) + T_o(\mathbf{x})$.

By applying the determinant operator to these tensors and by embedding these responses according to

$$\mathbf{d}_e = \det(T_e)\mathbf{e}_3 = A\mathbf{e}_3 \tag{64}$$

$$\mathbf{d}_o = \mathbf{e}_1 \det(T_o) = B\mathbf{e}_1 + C\mathbf{e}_2 \tag{65}$$

into $\mathbb{R}_3$, we follow the line drawn by the signal embedding sketched in section 4.3. This results in a novel signal representation which is called the generalized monogenic curvature signal

$$\mathbf{f}_{i2D}(\mathbf{x}) = \mathbf{d}_e(\mathbf{x}) + \mathbf{d}_o(\mathbf{x}). \tag{66}$$

The generalized monogenic curvature signal is a generalized monogenic representation of the Gaussian curvature in classical differential geometry. Because for i0D and i1D structures the determinants of the curvature tensor must be zero, any $|\mathbf{f}_{i2D}| > 0$ indicates an i2D structure. In the case of an i1D structure, the trace operator on the curvature tensors results in a signal model, which corresponds to the mean curvature in classical differential geometry,

$$\mathbf{f}_{i1D}(\mathbf{x}) = \text{ trace } (T_e) + \text{ trace } (T_o)\mathbf{e}_2 = \mathbf{f}(\mathbf{x}) + (r_2 * \mathbf{f})(\mathbf{x}). \tag{67}$$

Hence, in the case of $|\mathbf{f}_{i1D}| > 0$, this signal model is identical to the monogenic signal, equation (48). And vice versa, we can conclude that the monogenic signal is a monogenic measure of the mean curvature.

Interestingly, equation (66) may also be written as

$$\mathbf{f}_{i2D}(\mathbf{x}) = \mathbf{d}_e(\mathbf{x}) + \left(g_s^{(2)} * \mathbf{d}_e\right)(\mathbf{x}), \tag{68}$$

and it can be shown that $|\mathbf{d}_e| = |\mathbf{d}_o|$. This equation indicates that a generalized Hilbert transform, which equals a second order spherical harmonic, $g_s^{(2)}$, delivers the odd part of the monogenic curvature signal from the even one. It has been proved in [4] that the second order spherical harmonic represents also a valid generalization of the Hilbert transform. We therefore call the novel signal representation $\mathbf{f}_{i2D}$ generalized monogenic.

From the generalized monogenic curvature signal, local spectral representations of i2D structures can be computed in a similar way as from the monogenic mean curvature (monogenic signal). But details should be skipped here. Instead, it should be mentioned that as generalization of the monogenic scale-space, see sections 4.2 and 4.4, a generalized monogenic curvature scale-space [51] can be formulated that is defined as

$$\mathbf{f}_{i2D}^{s}(\mathbf{x}, s) = \mathbf{d}_e(\mathbf{x}, s) + \mathbf{d}_o(\mathbf{x}, s). \tag{69}$$

In the following two figures we want to give some simple demonstrations for the generalized monogenic curvature signal. Figure 4 shows to the left the original pattern and to the right the energy image. The response has the requested rotation invariance. Finally, in figure 5 we see to the left the original pattern and to the right the image of the i2D phase.

5. **Conclusions.** In this paper we reported on the generalization of the analytic signal to the monogenic one with respect to the dimension of the signal. This will give access to a complete local structure analysis in the nD case. By evaluating the local amplitude, phase and orientation, we have the possibility of characterizing the local signal dynamics, its symmetry, and its geometric embedding. Because the monogenic signal in the presented approach can be extended to a monogenic scale-space, all these quantities have to be understood as scale dependent. The approach establishes a unique embedding of these quantities in a linear scale-space theory based on the Poisson kernel and on the Riesz transform. The presented generalization works in a methodical stringent sense in the case of i1D structures. Its generalization to i2D structures is not generally possible. But there are ways to attack also such problems for special cases. Especially, considering the local curvature model in differential geometry, results in a monogenic curvature tensor representation which covers all intrinsic dimensions of 2D signals. We did not report on applications in depth. But over the years there have been a lot of them. We recommend the reader the website "http://www.ks.informatik.uni-kiel.de" for more details.

Acknowledgements. This work has been granted by DFG grants So-320/2-3 and So-320/4-2 (GS) and DFG Graduiertenkolleg No. 357 (DZ). The extension of the monogenic signal to 3D has been done by Martin Krause based on the EC grant IST-2001-34220 (VISATEC project). The authors' gratitudes to Michael Felsberg concern his fruitful work and stimulating discussions during the time of preparing his PhD thesis in the research group Cognitive Systems.

REFERENCES

1. N.H. Asmar, *Applied complex analysis with partial differential equations*, Prentice Hall, Upper Saddle River, 2002.
2. D. Boukerroui, J.A. Noble, and M. Brady, *On the choice of band-pass quadrature filters*, Journ. of Math. Imaging and Vision **21** (2004), 53–80.
3. F. Brackx, R. Delanghe, and F. Sommen, *Clifford analysis*, Pittman, Boston, 1982.
4. F. Brackx, B.D. Knock, and H.D. Schepper, *Generalized multidimensional Hilbert transforms in Clifford analysis*, International Journal of Mathematics and Mathematical Sciences **2006** (2006), Article ID 98145, 19 pages, doi:10.1155/IJMMS/2006/98145.
5. T. Bülow, M. Felsberg, and G. Sommer, *Non-commutative hypercomplex Fourier transforms of multidimensional signals*, Geometric Computing with Clifford Algebras (G. Sommer, ed.), Springer-Verlag, Heidelberg, 2001, pp. 187–208.
6. T. Bülow and G. Sommer, *The hypercomplex signal - a novel approach to the multidimensional analytic signal*, IEEE Trans. Signal Process. **49** (2001), no. 11, 2844–2852.
7. ———, *Local hypercomplex signal representations and applications*, Geometric Computing with Clifford Algebras (G. Sommer, ed.), Springer-Verlag, Heidelberg, 2001, pp. 255–289.
8. A.P. Calderón and A. Zygmund, *On the existence of certain singular integrals*, Acta Mathematica **88** (1952), 85–139.
9. R. Delanghe, F. Sommen, and V. Souček, *Clifford algebra and spinor valued functions*, Kluwer Academic Publishers, Dordrecht, 1992.
10. R. Duits, M. Felsberg, L. Florack, and B. Platel, *α scale spaces on a bounded domain*, Scale-Space 2003 (L.D. Griffin and M. Lillholm, eds.), LNCS, vol. 2695, Springer-Verlag, Berlin, Heidelberg, 2003, pp. 494–510.
11. R. Duits, L.M.J. Florack, J. de Graaf, and B.M. ter Haar Romeny, *On the axioms of scale-space theory*, Journal Math. Imaging and Vision **20** (2004), no. 3, 267–298.
12. J. Ebeling and G. Scheuermann, *Clifford Fourier transform on vector fields*, IEEE Trans. Visualization and Computer Graphics **11** (2005), no. 4, 469–479.
13. M. Felsberg, *Low-level image processing with the structure multivector*, Tech. Report No. 2016, Christian-Albrechts-Universität zu Kiel, Institut für Informatik und Praktische Mathematik, 2002.
14. ———, *On the design of two-dimensional polar separable filters*, EUSIPCO 2004, Proc. 12th European Signal Processing Conf., Vienna, 2004, pp. 417–420.
15. M. Felsberg, R. Duits, and L. Florack, *The monogenic scale-space on a bounded domain and its applications*, Scale-Space 2003 (L.D. Griffin and M. Lillholm, eds.), LNCS, vol. 2695, Springer-Verlag, Berlin, Heidelberg, 2003, pp. 209–224.
16. M. Felsberg and G. Sommer, *The monogenic signal*, IEEE Trans. Signal Process. **49** (2001), no. 12, 3136–3144.
17. ———, *Scale adaptive filtering derived from the Laplace equation*, 23. Symposium für Mustererkennung, DAGM 2001, München (B. Radig and S. Florczyk, eds.), LNCS, vol. 2191, Springer-Verlag, 2001, pp. 124–131.
18. ———, *The Poisson scale-space: A unified approach to phase-based image processing in scale-space*, Tech. Report No. 0208, Christian-Albrechts-Universit zu Kiel, Institut fr Informatik und Praktische Mathematik, August 2002.
19. ———, *The structure multivector*, Applications of Geometric Algebra in Computer Science and Engineering (L. Dorst, C. Doran, and J. Lasenby, eds.), Proc. AGACSE 2001, Cambridge, UK, Birkhäuser Boston, 2002, pp. 437–448.
20. ———, *The monogenic scale-space: a unifying approach to phase-based image processing in scale-space*, J. Math. Imag. and Vision **21** (2004), 5–26.
21. T.C. Folsom and R.B. Pinter, *Primitive features by steering, quadrature, and scale*, IEEE Trans. Patt. Anal. Mach. Intell. **20** (1998), no. 11, 1161–1173.
22. W.T. Freeman and E.H. Adelson, *The design and use of steerable filters for image analysis*, IEEE Trans. Patt. Anal. Mach. Intell. **13** (1991), no. 9, 891–906.
23. D. Gabor, *Theory of communication*, Journal of the IEE **93** (1946), 429–457.
24. G.H. Granlund and H. Knutsson, *Signal processing for computer vision*, Kluwer Academic Publishers, Dordrecht, 1995.
25. S.L. Hahn, *Hilbert transforms in signal processing*, Artech House, Boston, London, 1996.

26. D. Hestenes, H. Li, and A. Rockwood, *New algebraic tools for classical geometry*, Geometric Computing with Clifford Algebras (G. Sommer, ed.), Springer-Verlag, Heidelberg, 2001, pp. 3–26.
27. D. Hestenes and G. Sobczyk, *Clifford algebra to geometric calculus*, Reidel, Dordrecht, 1984.
28. A. Heyking and H. Freudenthal, *Collected works of l.e.j. brouwer*, North Holland Elsevier, New York, 1975.
29. T. Iijima, *Basic theory on normalization of patterns*, Bull. Electrotechnical Lab. **26** (1962), 368–388.
30. M. Krause and G. Sommer, *A 3d isotropic quadrature filter for motion estimation problems*, Conference Visual Communications and Image Processing, Beijing, China (S. Li, F. Pereira, H.-Y. Shum, and A.G. Tescher, eds.), SPIE, vol. 5960, The International Society for Optical Engineering, Bellingham, 2005, pp. 1295–1306.
31. G. Krieger and C. Zetzsche, *Nonlinear operators for the evaluation of local intrinsic dimensionality*, IEEE Trans. Image Processing **5** (1996), no. 6, 1026–1042.
32. C. Li, A. McIntosh, and T. Qian, *Clifford algebras, Fourier transforms, and singular convolution operators on Lipschitz surfaces*, Revista Matemática Iberoamericana **10** (1994), no. 3, 665–721.
33. T. Lindeberg, *Scale-space theory in computer vision*, Kluwer Academic Publ., Boston, 1994.
34. P. Lounesto, *Clifford algebras and spinors*, London Math. Soc. Lecture Note Ser., vol. 239, Cambridge University Press, 1997.
35. Y. Meyer and R. Coifman, *Wavelets: Calderón-zygmund and multilinear operators*, Cambridge University Press, 1997.
36. M. Michaelis and G. Sommer, *A Lie group approach to steerable filters*, Patt. Recogn. Lett. **16** (1995), 1165–1174.
37. A. Papoulis, *The fourier integral and its applications*, McGrau-Hill, New York, 1962.
38. E.J. Pauwels, L.J. van Gool, P. Fiddelaers, and T. Moons, *An extended class of scale-invariant and recursive scale space filters*, IEEE Trans. Patt. Anal. Mach. Intell. **17** (1995), no. 7, 691–701.
39. P. Perona, *Steerable-scalable kernels for edge detection and junction analysis*, Computer Vision - ECCV'92 (G. Sandini, ed.), LNCS, vol. 588, Springer-Verlag, Berlin, Heidelberg, 1992, pp. 3–18.
40. T. Qian and F. Sommen, *Deriving harmonic functions in higher dimensional spaces*, Journal for Analysis and its Applications **22** (2003), 275–288.
41. J. Radon, *On the determination of functions from their integral values along certain manifolds. (Translation of the original German text by P.C. Parks)*, IEEE Trans. Medical Imaging **5** (1986), no. 4, 170–176.
42. B. Rosenhahn and G. Sommer, *Pose estimation in conformal geometric algebra. PartI: Stratification of mathematical spaces*, Journ. Math. Imaging and Vision **22** (2005), 27–48.
43. G. Sommer (ed.), *Geometric computing with clifford algebras*, Springer-Verlag, Heidelberg, 2001.
44. G. Sommer, M. Michaelis, and R. Herpers, *The SVD approach for steerable filter design*, Proc. Int. Symp. on Circuits and Systems, vol. 5, 1998, pp. 349–353.
45. E.M. Stein, *Harmonic analysis*, Princeton University Press, Princeton, New Jersey, 1993.
46. ———, *Singular integrals: The roles of Calderón and Zygmund*, Notices of the American Mathemat. Soc. **45** (1998), no. 9, 1130–1140.
47. E.M. Stein and G. Weiss, *Introduction to fourier analysis on euclidean spaces*, Princeton Univ. Press, Princeton, 1971.
48. W. Yu, K. Daniilidis, and G. Sommer, *Approximate orientation steerability based on angular Gaussians*, IEEE Trans. Image Process. **10** (2001), no. 2, 193–205.
49. D. Zang and G. Sommer, *Phase based image reconstruction in the monogenic scale space*, 26. Symposium für Mustererkennung, DAGM 2004, Tübingen (C.E. Rasmussen, H.H. Bülthoff, M.A. Giese, and B. Schölkopf, eds.), LNCS, vol. 3175, Springer-Verlag, Berlin, Heidelberg, 2004, pp. 171–178.
50. ———, *An operator for the analysis of superimposed intrinsically two dimensional patterns*, 12th International Workshop on Systems, Signals and Image Processing, Chalkida, Greece, 22.-24.9.05 (D.A. Karras, S. Voliotis, M. Rangoussi, and A. Kokkosis, eds.), Inderscience, Genève, 2005, pp. 77–81.

51. ———, *The monogenic curvature scale-space*, 11th International Workshop on Combinatorial Image Analysis, IWCIA'06, Berlin (R. Reulke, U. Eckardt, B. Flach, U. Knauer, and K. Polthier, eds.), LNCS, vol. 4040, Springer-Verlag, Berlin, Heidelberg, 2006, pp. 320–332.
52. ———, *Signal modeling for two-dimensional image structures*, Journal of Visual Communication and Image Representation **18** (2007), no. 1, 81–99.
53. C. Zetzsche and E. Barth, *Fundamental limits of linear filters in the visual processing of two-dimensional signals*, Vision Research **30** (1990), 1111–1117.

Received September 15, 2005; revised February 2007.

E-mail address: {gs,zd}@ks.informatik.uni-kiel.de